AMERICAN SOCIETY FOR MICROBIOLOGY | Applied and Environmental Microbiology®

MINIREVIEW

Microbially Induced Calcium Carbonate Precipitation by *Sporosarcina pasteurii*: a Case Study in Optimizing Biological $CaCO_3$ Precipitation

Michael S. Carter,[a,b] Matthew J. Tuttle,[a,b] Joshua A. Mancini,[a,b] Rhett Martineau,[a,b] Chia-Suei Hung,[a] Maneesh K. Gupta[a]

[a]Materials and Manufacturing Directorate Air Force Research Lab, Wright-Patterson Air Force Base, Dayton, Ohio, USA
[b]Biological and Nanoscale Technologies Division, UES, Inc., Dayton, Ohio, USA

ABSTRACT Current production of traditional concrete requires enormous energy investment that accounts for approximately 5 to 8% of the world's annual CO_2 production. Biocement is a building material that is already in industrial use and has the potential to rival traditional concrete as a more convenient and more environmentally friendly alternative. Biocement relies on biological structures (enzymes, cells, and/or cellular superstructures) to mineralize and bind particles in aggregate materials (e.g., sand and soil particles). *Sporosarcina pasteurii* is a workhorse organism for biocementation, but most research to date has focused on *S. pasteurii* as a building material rather than a biological system. In this review, we synthesize available materials science, microbiology, biochemistry, and cell biology evidence regarding biological $CaCO_3$ precipitation and the role of microbes in microbially induced calcium carbonate precipitation (MICP) with a focus on *S. pasteurii*. Based on the available information, we provide a model that describes the molecular and cellular processes involved in converting feedstock material (urea and Ca^{2+}) into cement. The model provides a foundational framework that we use to highlight particular targets for researchers as they proceed into optimizing the biology of MICP for biocement production.

KEYWORDS MICP, *Sporosarcina pasteurii*, biocementation, calcium carbonate, urease, microbially induced calcium carbonate precipitation, biocement

Portland cement has been in use since the 1820s as the agent that binds aggregate materials to form concrete (1). Portland cement is produced by heating lime and clay to temperatures over 1400°C. Contemporary cement production methods account for ~0.6% of U.S. energy consumption and contribute to approximately 5 to 8% of the world's CO_2 emissions (1–3). The result is a product that develops cracks that can be filled but never truly repaired.

Biocement is a material that relies on biological structures (enzymes, cells, and/or cellular superstructures) to bind aggregates (e.g., sand and soil particles). Biocement production requires less energy than traditional concrete and offers the potential for self-repair (4). Biocementation strategies are commonly versions of microbially induced $CaCO_3$ precipitation (MICP) where the generated $CaCO_3$ crystals bind aggregates into a structurally robust material (Fig. 1). Current investigations are considering biocement for processes such as stabilizing drilling wells (5, 6), stabilizing loose soils (7–9), and producing environmentally friendly building materials (10).

MICP is commonly separated into two categories (nonureolytic and ureolytic) that each rely on exogenously provided sources of Ca^{2+} and CO_3^{2-}. Ureolytic MICP relies on urease-producing microbes to hydrolyze urea into NH_3 and H_2CO_3. The generated NH_3 causes the environment to become more basic, which favors formation of $CaCO_3$ from the interaction of CO_3^{2-} and Ca^{2+}.

Editor Arpita Bose, Washington University in St. Louis

Address correspondence to Maneesh K. Gupta, maneesh.gupta.2@us.af.mil.

The authors declare no conflict of interest.

Published 13 July 2023

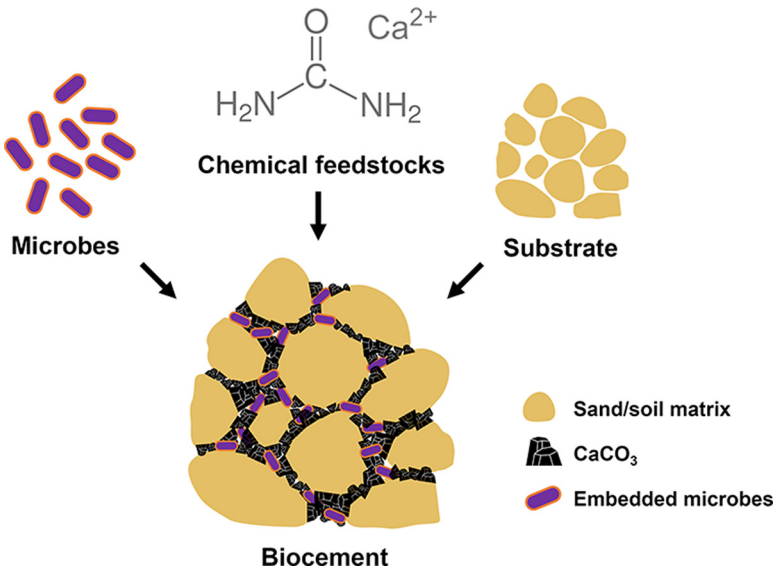

FIG 1 Biocement formation via ureolytic MICP. Microbial metabolism consumes urea to generate products that induce formation of $CaCO_3$ that cements substrates into a more rigid material.

Efforts are under way to improve $CaCO_3$ precipitation in MICP to produce commercially viable replacements for contemporary concrete. Common commercial biocement processes rely on the ureolytic bacterium *Sporosarcina pasteurii* (previously *Bacillus pasteurii*) because the bacterium produces high urease activity, grows best at elevated pH values, and has a high tolerance for elevated concentrations of NH_3 and salts (11, 12).

Because previous reviews have broadly described organisms and molecular mechanisms related to ureolytic and nonureolytic MICP (13, 14), we present a focused discussion on relevant properties of bacteria in MICP, specifically *S. pasteurii*. We offer a model (Fig. 2) that highlights the current molecular and cellular understanding of ureolytic MICP and identifies potential bioengineering and synthetic biology targets for improving MICP.

MICROBES THAT CAN INDUCE $CaCO_3$ PRECIPITATION

MICP is a common biogeochemical process in varied environments, including soils, caves, freshwater and marine sediments, oceans, and lakes (freshwater, saline, and alkaline) (15–19). MICP-relevant microbes can employ an array of metabolisms that are categorized into two general groups: ureolytic and nonureolytic. Ureolytic MICP relies on enzymatic hydrolysis of urea and is the best-studied mechanism of MICP, especially in applied research (20, 21). Nonureolytic MICP includes a broader range of metabolisms such as nitrogen fixation, ammonification, denitrification, dissimilatory sulfate reduction, and photosynthesis (13, 14).

MICP can be implemented via bioaugmentation (exogenous addition of organisms) or biostimulation (employing endogenous organisms). Bioaugmentation usually involves a single organism chosen for a specific application. Examples include *S. pasteurii* application to seal oil field wellbores, *Exiguobacterium mexicanum* isolated from seawater for marine concrete remediation, and ureolytic bacteria from a South Korea metal mine for lead bioremediation (6, 22, 23). Biostimulation is used to prevent erosion of nutrient-poor soils and to increase strength of natural construction materials such as rammed earth (24–26). Dhami et al. concluded that biostimulation was favored at sites with high organic carbon content, while bioaugmentation was favored when treating nutrient-poor soils (27).

Photosynthetic microbes such as cyanobacteria and eukaryotic microalgae (e.g., coccolithophores), although infrequently employed for MICP, commonly form complex geological structures such as stromatolites and other microbialites (28, 29). Coccolithophores (a type of eukaryotic phytoplankton) form scale-like $CaCO_3$ plates around single cells and have been observed in geologic deposits dating to the Late Triassic (30). Although photosynthetically driven MICP might be difficult to harness, this process could be promising in an MICP consortium.

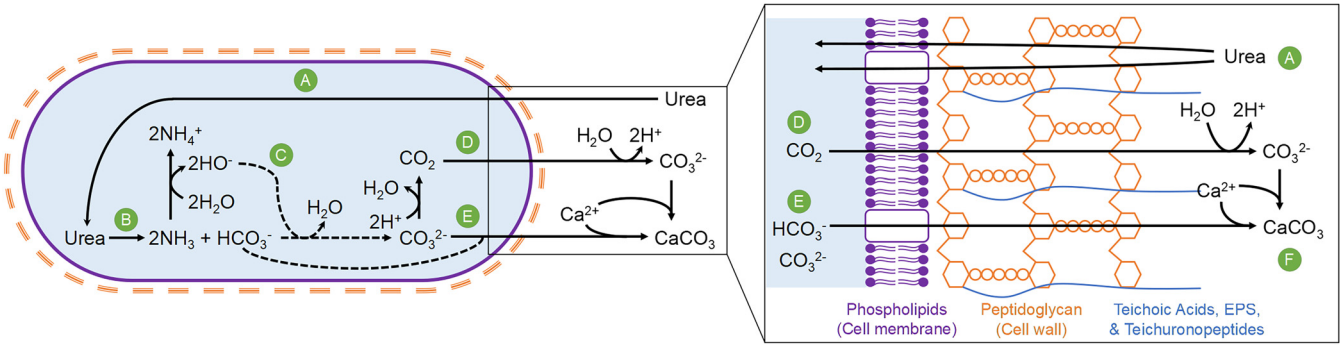

FIG 2 Current model of cellular structures and processes involved in ureolytic $CaCO_3$ precipitation by *S. pasteurii*. (A) Urea enters the cell through a transporter or via diffusion through the membrane. (B) Urease catalyzes hydrolysis of urea into NH_3 and H_2CO_3, which is equilibrated to HCO_3^- at physiological pH. (C) Ammonia collects protons from the environment (H_2O), generating a basic environment (–OH) that deprotonates a proportion of the HCO_3^- to CO_3^{2-}. The resulting HCO_3^-/CO_3^{2-} exits the cell in one of two ways (D or E). (D) HCO_3^-/CO_3^{2-} is temporarily dehydrated to form CO_2 via carbonic anhydrase activity. The CO_2 diffuses through the cell membrane and is spontaneously rehydrated and deprotonated by the basic environment to reform HCO_3^-/CO_3^{2-} is transported across the cell membrane. (F) Ca^{2+} that is concentrated outside of the cell via interactions with extracellular structures such as teichoic acids, teichuronopeptides (TUPs), and extracellular polymeric substances (EPS) rapidly interacts with CO_3^{2-} to form $CaCO_3$. As CO_3^{2-} is consumed, CO_3^{2-} is spontaneously equilibrated to generate more CO_3^{2-} for additional $CaCO_3$ formation.

Isolated from soil and sewage as a spore-forming alkaliphile with high urease activity, *Sporosarcina pasteurii* is the model system for MICP (20, 21, 31, 32). The MICP community employs multiple strains of *S. pasteurii* (i.e., DSM 33, BNCC 337394, ATCC 6453, and MTCC 1761), depending on the researchers' preferred culture collection (12, 33). MICP via *S. pasteurii* occurs rapidly in many soil types and, with the exception of Mg^{2+}, is largely independent of low concentrations of cations other than the requisite Ca^{2+} (34). Efforts to optimize growth of and cementation by *S. pasteurii* will be discussed briefly below, but more details have been extensively reviewed elsewhere (12, 20, 21, 35–38).

Ureolytic MICP has also been investigated in other species, including *Sporosarcina ureae*, undesignated *Sporosarcina* spp., and close relatives of *Sporosarcina* (39–42). *Bacillus cereus*, *Bacillus licheniformis*, *Priestia megaterium* (formerly *Bacillus megaterium*), and *Lysinibacillus sphaericus* (formerly *Bacillus sphaericus*) are ureolytic and tolerate high pH (18, 43–48). *Bacillus subtilis*, *Bacillus mucilaginousm*, *Bacillus cohnii*, and *Bacillus pseudofirmus* have been used to improve the structure and strength of sand and soil in nonureolytic MICP (49–56). Notably, a genetically engineered strain of *B. subtilis* capable of ureolytic MICP was recently investigated (see below) (14).

While environmental MICP is commonly attributed to bacteria, recent evidence recognizes significant fungal contributions (57, 58). Recent studies suggest that urease-positive fungi (i.e., *Neurospora crassa*, *Pestalotiopsis* sp., *Myrothecium gramineum*, *Colletotrichum acutatum*, *Penicillium chrysogenum*, *Fusarium cerealis*, *Phoma herbarum*, and *Mucor hiemalis*) can also form biocement (59–64). Fungal mycelia might provide structure and strength to biocements (57).

CELLULAR ANATOMY AND PHYSIOLOGY INVOLVED IN UREOLYTIC $CaCO_3$ PRECIPITATION

Ureolytic cementation minimally requires urease activity but is enhanced by intact cells (14, 65, 66). The following section discusses MICP-relevant cellular processes and structures while highlighting detailed information that is currently available for *S. pasteurii*.

Path of urea through an *S. pasteurii* cell during MICP. For ureolytic MICP, urea must be imported and hydrolyzed before CO_3^{2-} can be released to interact with extracellular Ca^{2+} (Fig. 2). Urea transport in bacteria has been observed via urea channels and active transporters (67–69). Although channels can be gated, channels cannot concentrate urea inside of a cell as is possible with active transporters. We were unable to find reports of urea channels or transporters in *S. pasteurii*.

Once inside, urea is hydrolyzed by the cytoplasmic enzyme urease. For 1 mol urea, urease releases 1 mol of $H_2CO_3/HCO_3^-/CO_3^{2-}$ (pK_{a1} ~3.5 [70], pK_{a2} ~10) and 2 mol of NH_3 (71) (Fig. 2B). The NH_3 rapidly collects protons, increasing the local pH. Upon sustained urea

hydrolysis, the environmental pH eventually reaches ~9.2, the pK_a for the proton on NH_4^+ (72) and a suitable pH for *S. pasteurii* growth (12).

To maintain an internal pH of 6.0 to 8.5, *S. pasteurii* cells likely use a combination of strategies, including uncharacterized NH_4^+ export that enables net movement of H^+ into the cell (73, 74). The differential pH of the interior and exterior of the cell impacts options for exporting HCO_3^- and the equilibrium experienced among CO_2, HCO_3^-, and CO_3^{2-}, which shifts toward CO_3^{2-} as pH increases. Given the charge on HCO_3^- and CO_3^{2-}, neither molecule can be exported without a transporter (75). *S. pasteurii* likely manages excess HCO_3^-/CO_3^{2-} via some combination of two strategies: (i) dehydration of HCO_3^- to CO_2 or (ii) export of HCO_3^-/CO_3^{2-} (Fig. 2D or E).

With the first strategy, carbonic anhydrase might catalyze reversible dehydration of HCO_3^- to generate CO_2, which easily diffuses across biological membranes (75). Once outside of the cell, a proportion of the CO_2 is rehydrated and/or deprotonated to form HCO_3^-/CO_3^{2-} (Fig. 2D). Although the involvement of carbonic anhydrase in MICP is unstudied in *S. pasteurii*, a carbonic anhydrase gene is present in *S. pasteurii* BNCC 337394 (33), and the role of carbonic anhydrase is well established in biological $CaCO_3$ precipitation (27, 76–78).

In the second strategy, HCO_3^-/CO_3^{2-} might be exported by *S. pasteurii* (Fig. 2E). Throughout the process described in Fig. 2, the proportion of protonated and deprotonated CO_3^{2-} shifts with the ever-changing pH as ureolysis continues. Inside the cell where the pH is relatively constant, HCO_3^- is likely the primary form. Although import of HCO_3^- is well known in cyanobacterial carbon concentration mechanisms and HCO_3^- export is well studied in human cells, we found no reports of HCO_3^- export in bacteria (79, 80).

Role of cell surface structures in MICP. Despite rapid intracellular production of HCO_3^- in *S. pasteurii* during ureolysis, $CaCO_3$ precipitation likely does not occur until CO_3^{2-} is present outside the cell (Fig. 2F). Independent of extracellular Ca^{2+} concentrations, intracellular Ca^{2+} concentrations are typically no higher than 4 μM in bacteria (81, 82). In addition, there is evidence from work with *S. pasteurii* and closely related bacteria that extracellular structures drive $CaCO_3$ precipitation. For *B. subtilis* 168, deletion of genes involved in producing extracellular structures (teichoic acids and spore coat constituents) reduces $CaCO_3$ precipitation efficiency (83). For *P. megaterium* and *S. pasteurii*, $CaCO_3$ precipitation was observed to correlate with the presence of extracellular polymeric substances (EPS; biofilm matrix components), and purified EPS from two environmental bacterial strains were observed to increase $CaCO_3$ precipitation *in vitro* (84–86).

EPS are often negatively charged structures (DNA and proteins) and hydrophilic polysaccharides (87). Cell walls of Gram-positive alkaliphiles also include negatively charged teichoic acids and teichuronopeptides (TUPs). TUPs are unique to alkaliphiles and serve to concentrate H^+ at the cell surface for use in oxidative phosphorylation (88), which is particularly challenging in alkaline conditions (see below). Similarly, the collection of fully and partially negatively charged components likely concentrates Ca^{2+} ions for rapid $CaCO_3$ precipitation at the cell surface as CO_3- is released from the cell (Fig. 2F and Fig. 3) (89).

Ma et al. investigated the outer structures of *S. pasteurii* BNC 337394 cells during growth in rich media with or without added urea (33). In the absence of urea, Ma et al. observed the following for *S. pasteurii*: (i) genes for aerobic respiration (electron transport chain proteins and ATP synthase) were upregulated, (ii) fewer cells developed, (iii) cells were deformed with a less negative zeta potential on the outer surface, and (iv) cells were less effective at biocementation. Williams et al. also measured zeta potential of *S. pasteurii* (ATCC 6453) in various urea-containing rich media and observed that in the presence of urea the zeta potential of cells was substantially negative (ca. –35 mV) (38). Ma et al. observed the aforementioned regulation via transcriptomics, but the researchers did not report whether their transcriptome data correlated with their observations related to cellular anatomy and physiology.

Role of urea and NH_4^+ in *S. pasteurii* physiology. Inside *S. pasteurii* cells grown with urea, high urease activity offers access to NH_4^+ ions for adjusting essential physiological characteristics. Early studies isolated and defined strains of *S. pasteurii* based on

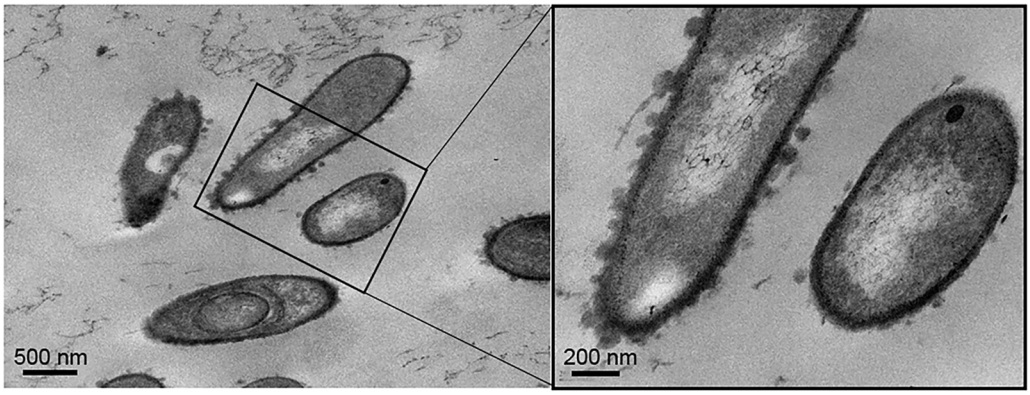

FIG 3 Transmission electron micrographs of *S. pasteurii* cells with surface affixed $CaCO_3$ crystals. Cells were grown for up to 7 days at 30°C as a stab culture in a semisolid (0.5% agar) pH 7 medium that contained 2% urea, 0.15% peptone, 0.09% beef extract, 0.06% sodium chloride, and 0.28% $CaCl_2$. The surface crystals were identified as $CaCO_3$ via combinations of scanning and transmission electron microscopy, energy dispersive X-ray spectroscopy (EDS), and X-ray powder diffraction (XRD). (Reproduced from reference 89.)

requirements for high concentrations of ammonium for optimal growth and for growth in urea-rich media (90–92). Indeed, reports have historically claimed that *S. pasteurii* can only grow with media that contains urea (91, 93). More recent reports, however, have observed that urea is not required, particularly in media with elevated pH (33, 34).

At cytoplasmic pH, nearly all of urease-generated NH_3 is in the form of NH_4^+. Rather than the toxicity that other nonbacterial cells experience (94–96), *S. pasteurii* grows well in media with up to 330 mM urea (38, 97), which if completely hydrolyzed would release 660 mM NH_4^+. We were unable to find any studies that report the quantitative effects of elevated NH_3/NH_4^+ levels on *S. pasteurii* growth, but *S. pasteurii* cells have been qualitatively observed to grow in NH_3/NH_4^+ concentrations up to 500 mM (11).

Evidence suggests that during growth with urea, *S. pasteurii* uses NH_4^+ to maintain a physiologically necessary lower intracellular pH compared to the elevated extracellular pH (73). Alkaliphiles like *S. pasteurii* commonly keep their intracellular pH lower than the alkaline environment by accumulating positive ions intracellularly (e.g., Na^+ or K^+ [98]) to exchange for protons from the environment. Jahns observed that in conditions that imitate growth in media with high urea concentrations, intracellular NH_4^+ concentrations in *S. pasteurii* were up to 30-fold higher than extracellular concentrations (73).

Given the inverted pH difference between the inside and outside of cells in alkaline environments, alkaliphilic aerobes must have strategies for maintaining a proton flow through respiratory ATPases. Jahns suggested that *S. pasteurii* might use NH_4^+ accumulation as a strategy for managing the proton potential at the membrane without changing the intracellular pH (73). Evidence suggests that *S. pasteurii* and other alkaliphiles use a strongly negatively charged cell surface to concentrate protons immediately outside the cytoplasm (73, 88, 99).

NH_4^+ is also a common N-source among organisms, but perhaps not for *S. pasteurii*. Early descriptions of *S. pasteurii* noted no observable glutamine synthetase activity (for high efficiency NH_4^+ assimilation) and low glutamate dehydrogenase activity (for low-efficiency NH_4^+ assimilation) in extracts of cells regardless of whether NH_4^+ was included in the rich growth medium (100). Indeed, in rich media that contained urea or NH_4^+, more NH_4^+ was detectable after growth than was initially added as urea or NH_4^+.

Lapierre et al. investigated the requirements in a defined medium for growth of *S. pasteurii* DSM 33 and observed that the growth rate and yield of *S. pasteurii* cultures were independent of whether $(NH_4)_2SO_4$ was excluded or provided at double concentrations in media that contained urea (12). The authors did not report growth data in the absence of urea, but the authors observed that addition of amino acids derived from glutamate, including arginine whose degradation can generate urea, increased growth rate and growth yield.

GENETIC APPROACHES TO OPTIMIZE MICP

Most of the work on MICP to date has been performed by civil and materials engineering research groups that have identified conditions in which MICP is effective. Only more recently have these and other researchers begun to employ genetic engineering strategies to investigate how cells can be modified to improve MICP efficiency. Early studies include UV mutagenesis of *S. pasteurii* MTCC 1761. Only some mutagenized strains with elevated urease activity induced greater $CaCO_3$ precipitation, but all strains that induced greater $CaCO_3$ precipitation also produced excess EPS (84).

Without a genetic toolbox, other genetic approaches in *S. pasteurii* are currently limited. Instead, researchers have moved MICP-related genes into organisms with abundant tools. Liang et al. inserted various urease gene clusters into *Escherichia coli* and observed that while urease gene cluster expression weakly correlated with $CaCO_3$ crystal size, urease activity inversely correlated with crystal size (101, 102).

Instead of engineering *E. coli*, which is evolutionarily distinct from *S. pasteurii*, other research groups have modified *B. subtilis*, a closer evolutionary relative of *S. pasteurii*. Hoffman et al. identified that $CaCO_3$ precipitation was induced best in *B. subtilis* strains that were (i) grown in biofilm-promoting conditions, (ii) contained urea transporters, and (iii) contained the urease gene cluster from *B. paralicheniformis* rather than *S. pasteurii* (97). The researchers suggested that the difference in expression levels was due to the closer evolutionary relationship between *B. paralicheniformis* and *B. subtilis*.

ROLE OF UREASE IN MICP

Urease enzymes are cytoplasmic and commonly serve as components in nitrogen scavenging pathways, acid tolerance/alkalinization pathways, and virulence strategies (100, 103–105). Urease activity is a common characteristic used to clinically distinguish and identify bacterial pathogens such as *H. pylori* that adjust the environmental pH to better suit growth (105). This section will discuss the structure and operation of urease as a tool for MICP.

Properties of urease enzymes. Since urease from jack bean was the first enzyme to be crystallized (71), researchers have investigated ureases from various organisms to identify active site residues, Ni^{2+}-binding residues, inhibitors, subunit assembly schemes, and a variety of structural and regulatory schemes. For *S. pasteurii*, at the time of this writing, there are 32 independent Protein Database (PDB) entries of *S. pasteurii* wild-type urease enzymes with or without inhibitors or urea (106, 107).

While plant and animal ureases are commonly trimers or hexamers of a single polypeptide (~90 kDa), bacterial ureases are more commonly composed of three distinct subunits (α, β, and γ; ~90 kDa total) that assemble into a trimer of heterotrimers (108). In cases in which the subunits are not distinct polypeptides, including in plants and animals, the subunits are typically fused versions of the α, β, and/or γ subunits from the trimer variants. For example, the *S. pasteurii* urease is composed of three subunits (α, β, and γ), but the *H. pylori* urease is composed of two subunits. In *H. pylori*, the β (10 to 20 kDa in other organisms) and the γ subunits (9 to 14 kDa in other organisms) are effectively fused as a single 26.5-kDa subunit (108).

In all cases, urease is Ni^{2+} dependent, and the active site is in the α-subunit or equivalent region (108). Many organisms, including *S. pasteurii*, use accessory proteins (UreD, UreE, and UreF) to efficiently assemble the subunits and insert Ni^{2+} for holoenzyme formation (108). According to structures for ureases from *S. pasteurii* and *Klebsiella aerogenes*, the active sites contain two Ni^{2+} ions in coordination with a small set of lysine and histidine residues in a consistent coordination geometry (107, 109, 110). Often, the urease structural proteins and the accessory proteins are proximally encoded in likely operons. The genetic arrangement of *ure* genes in genomes and the structural arrangement of Ure proteins in ureases of various organisms are thoroughly reviewed by Krajewska et al. (108).

For *S. pasteurii* urease, observed K_m values for urea are variable but universally high. With partially purified free enzyme, researchers have measured K_m values of 17.3 mM (111), 40 mM (112), and 235 mM (113). For comparison, K_m values for ureases from *Enterobacter* sp.

and *H. pylori* are 0.0195 and 0.2 mM (114, 115). The optimal activity of *S. pasteurii* urease occurs at pH 8.0 with 20% of optimum activity at pH 6.5 and 9.0 (113). Researchers have reported V_{max} values for *S. pasteurii* urease, but meaningfully comparing the reported values is challenging because of variations in the levels of enzyme purity and the methods used for measuring activity (111, 116). Altogether, the *S. pasteurii* enzyme is limited in its ability to access low concentrations of urea and has a narrow pH range.

For the purpose of MICP, the effective urease activity of whole cells is most relevant. Lauchnor et al. used equivalent *S. pasteurii* cell numbers to inoculate sealed BHI cultures that contained various concentrations of urea. Based on urea consumption after 1 h of incubation, Lauchnor et al. estimated effective K_m values to be 300 to 360 mM. Lauchnor et al. also observed that whole-cell urease activity was independent of NH_4^+ concentrations (6 to 147 mM) or pH (5 to 10) in the medium, suggesting that the internal pH of *S. pasteurii* cells is largely unchanged relative to environmental pH. Unlike Lauchnor et al., other researchers accounted for changes in urea concentration over the span of their assays and estimated whole cell effective K_m values to be 45, 73, and 300 mM (117–119).

Regulation of urease. Given the array of physiological roles served by urease, regulation schemes vary among organisms and respond to multiple environmental signals. Often in bacteria that rely on urease for N-assimilation, expression of the *ure* genes is upregulated directly or indirectly by NtrC (a σ^{54}-dependent nitrogen regulatory protein). When other more favorable N sources are unavailable (120–123) urease activity responds to urea concentrations in addition to or instead of additional N-sources (104). In bacteria, activity of σ^{54} is typically regulated by N availability (124).

Regulation of *ure* gene expression in *Klebsiella aerogenes* and *B. subtilis* occurs at multiple promoters (125, 126). In *K. aerogenes*, *ure* genes are driven by a Nac-regulated σ^{70} promoter and a σ^{54} promoter. In *B. subtilis*, regulation of *ure* genes is tightly linked to N metabolism but seems independent of NtrC and σ^{54} (127). Instead, a collection of regulators involved in a variety of N-related metabolic regulation schemes also regulate at least one *ure* promoter. Although pathways regulated by the same regulators generate urea in *B. subtilis*, urease activity is related to NH_4^+ levels rather than urea levels (127).

Given the close evolutionary relationship between the *Bacillus* and *Sporosarcina* genera, insights from regulation in *Bacillus* species might provide insight into regulation in *S. pasteurii*. Current evidence suggests that urease activity in *S. pasteurii*, therefore *ure* gene expression, is constitutively high (>10,000 nmol/min/mg in cell extract) regardless of the presence of added urea or NH_4^+ in rich media (100). Whole-cell urease activity was also independent of the concentration of NH_4^+ included in rich media (116). In more variable conditions that include minimal and defined media, upregulation of urease activity was observed to be approximately 2- to 5-fold in response to addition of amino acids, particularly amino acids that are biological derivatives of glutamate (12). The aforementioned observations, however, do not account for metabolic regulation that regularly occurs in various growth phases.

Two studies have compared transcript levels of *ure* genes in *S. pasteurii* BNCC 337394 during growth in conditions with or without urea and NH_4^+. Ma et al. observed that during growth in rich media with urea, exponentially growing cells upregulated nearly all *ure* gene transcripts approximately 2- to 4-fold (33). Pei et al. observed approximately 2- to 16-fold upregulation of *ure* transcripts when NH_4^+ or urea was present in rich media but did not control for growth phase.

Much work has been focused on upregulating urease activity in *S. pasteurii*, assuming that increased urease activity will increase biocementation efficacy (84). Rather, Konstantinou et al. observed that cells with lower urease activity cemented samples more uniformly (Fig. 4).

ADDITIONAL BIOLOGICAL STRATEGIES FOR $CaCO_3$ PRECIPITATION

Effective strategies for MICP should be informed by $CaCO_3$ precipitation that occurs in higher organisms. In these organisms, $CaCO_3$ formation is often highly controlled, even to the level of crystal morphology. $CaCO_3$ exists in at least three crystal morphologies: rhombohedral calcite, fibrous aragonite, and spherical vaterite (Fig. 5) (128). Calcite and

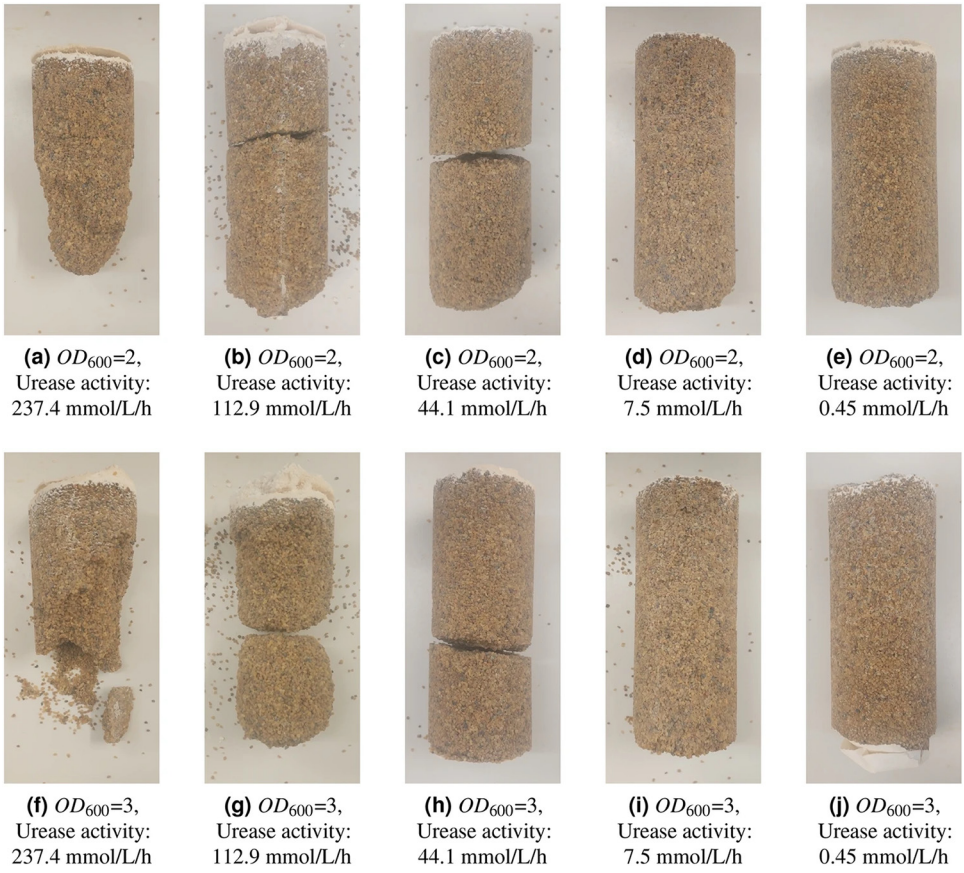

FIG 4 Qualitative observation of biocementation uniformity based on levels of urease activity. (a to e) Sand columns were biocemented with equivalent concentrations of cells (optical density at 600 nm [OD_{600}] = 2) with variable levels of urease activity in descending order 237.4, 112.9, 44.1, 7.5, and 0.45 mmol/L/h, respectively. (f to j) Sand columns were biocemented with equivalent concentrations of cells (OD_{600} = 3) with variable levels of urease activity in descending order as described below each photograph. Cells and cementation solutions were injected from top to bottom. (Reproduced from reference 165; see the reference for a quantitative analysis of cementation strength and uniformity of the columns.)

aragonite are the most commonly observed morphologies, whereas vaterite is a thermodynamically metastable state that ultimately leads to aragonite and calcite (128, 129).

In the case of *S. pasteurii* as modeled in Fig. 2, Ca^{2+} is concentrated at the cell surface, but the arrangement of Ca^{2+} ions relative to each other is not controlled. In the anatomy of structures from higher organisms, such as mollusk shells and egg shells, the formation of $CaCO_3$ must be tightly controlled in order to develop large-scale structures with consistent properties and a specific shape. In this section, we review proteins that have been observed *in vitro* to be involved in $CaCO_3$ precipitation in higher organisms.

Calcite-forming proteins. Calcite commonly develops from less ordered morphologies of $CaCO_3$ as biominerals cure. Early work reported that proteins found in biomineralized aragonite or calcite could form aragonite or calcite *in vitro* (129). Later work observed that the initial formation of mineralized $CaCO_3$ is commonly directed by an organic scaffold. Different proteins in the organic scaffold can impact the final morphology of the $CaCO_3$ mineral (Table 1) (129).

Reports about calcite-forming proteins primarily focus on proteins involved in avian egg shell production. In egg shells, hundreds of proteins are involved in nucleating calcite, increasing the concentration of calcium and carbonate near the nucleation site and assembling and orienting amorphous calcium carbonate to form calcite (77, 130–137). The best-studied proteins include ovalbumin, lysozyme, and ovotransferrin. The highly acidic ovalbumin alone *in vitro* binds to Ca^{2+}, which causes unfolding and allows interactions among unfolded ovalbumin molecules. Ovalbumin oligomers formed in this way enrich amorphous

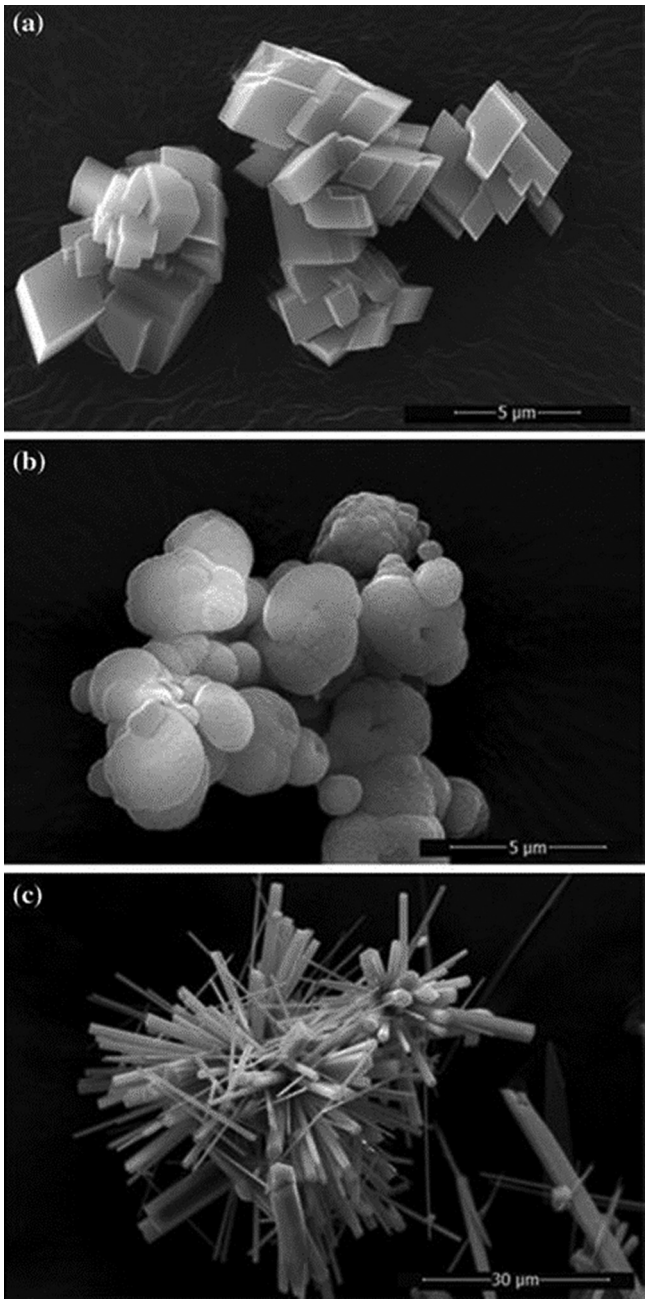

FIG 5 Crystal morphologies of $CaCO_3$. Images of calcite (a), vaterite (b), and aragonite (c) were collected by scanning electron microscopy. (Reproduced from reference 128 with permission from Spring Nature and Copyright Clearance Center.)

$CaCO_3$ (138–141). When the highly basic protein lysozyme is included with ovalbumin *in vitro*, the mix primarily drives formation of calcite (140, 142). Ovotransferrin is involved *in vivo* by directing mineralization to the outer egg shell membrane, potentially increasing calcite crystal size (143). The overall process of calcite formation and localization in egg shell formation is reviewed by Gautron et al. (77).

Reports of non-egg-shell proteins that can form calcite *in vitro* are rare and are primarily from organisms in marine environments where aragonite formation is more common. The proteins tend to be glycine-rich and rely on acidic residues such as glutamate and aspartate for Ca^{2+} binding (78, 144, 145).

Overall, strategies for calcite formation in higher organisms and $CaCO_3$ formation in MICP have parallel themes. Both strategies rely on negatively charged (acidic) molecules to collect

TABLE 1 Roles of select $CaCO_3$-forming proteins

Protein	Mol wt (kDa)[a]	Organism	$CaCO_3$ morphology	UniProt ID or reference
Pearlin	16.7	*Pinctada mazatlanica*	Aragonite	I2FK00
N14	13.7	*Pinctada maxima*	Aragonite	Q9NL39
N66	59.8	*Pinctada maxima*	Aragonite	Q9NL38
N16.3	12.9	*Pinctada fucata*	Aragonite	Q9TW98
PFMG1	13.6	*Pinctada fucata*	Aragonite	Q3YL59
Pif80	55	*Pinctada fucata*	Aragonite	C7G0B5
Pif97	59.8	*Pinctada fucata*	Aragonite	C7G0B5
N40	40	*Pinctada fucata*	Aragonite	161
Ps19	19	*Pteria sterna*	Aragonite	155
AP7	7.5	*Haliotis rufescens*	Aragonite	Q9BP37
Acid-rich protein 1	14	*Stylophora pistillata*	Aragonite	158
Acid-rich protein 2	18	*Stylophora pistillata*	Aragonite	158
Acid-rich protein 3	20	*Stylophora pistillata*	Aragonite	158
Acid-rich protein 4	37	*Stylophora pistillata*	Aragonite	158
Ovalbumin	42.7	*Gallus gallus*	Calcite	A0A411G5W6
Lysozyme	14.3	*Gallus gallus*	Calcite	P00698
GRP_BA	32.8	*Pinctada fucata*	Calcite	O02401
ECMP-67	67	*Lobophytum crassum*	Calcite	78

[a]Molecular weight does not include signal peptides.

Ca^{2+} and to provide sites for $CaCO_3$ nucleation. However, by incorporating lessons from higher organisms, MICP researchers can more precisely produce and place calcite, the strongest of the $CaCO_3$ morphologies.

Aragonite-forming proteins. Many more aragonite-forming than calcite-forming proteins have been isolated either from their source organism or from recombinant production. Aragonite-forming proteins are typically highly acidic and are often structurally disordered (146, 147). The most studied proteins that catalyze aragonite formation come from mollusks and often require chitin binding for activity. Due to their interaction with insoluble chitin fibers, the proteins are designated as insoluble shell matrix or framework proteins (148). While many nacre shell matrix proteins have been described, only a subset has been observed to form aragonite *in vitro*.

Members of the aragonite-forming fN14/N16/pearlin protein family are small disordered proteins that contain four acidic domains, an NG repeat domain, and a series of conserved cysteine residues (149). The family members are generally disordered until binding Ca^{2+} when they likely oligomerize to form a gel-like matrix scaffold (150). Examples include proteins from pearl oysters such as the glycosylated pearlin (16.7 kDa) from *Pinctada mazatlanica*, N16 (12.9 kDa) and PFMG1 (13.6 kDa) from *Pinctada fucata*, and a combination of N14 (13.7 kDa; homolog of N16) and N66 (59.8 kDa) from *Pinctada maxima* (149, 151). The morphology of the $CaCO_3$ formed by the proteins can be adaptable, depending on the presence of $CaCl_2$ and $MgCl_2$ (aragonite formation) or only $CaCl_2$ (calcite formation) (150, 152–154). Also, some of the proteins, although already small, can be further minimized to only two 30-residue fragments from each terminus of the given protein (154).

Other small disordered aragonite-forming proteins outside the fN14/N16/pearlin protein family include Ps19 (19 kDa) from the less studied pearl oyster *Pteria sterna*, AP7 (7.5 kDa) from pacific red abalone (*Haliotis rufescens*), and four acid-rich proteins (14, 20, 18, and 37 kDa) from the stony coral *Stylophora pistillata*. Ps19 is a glycoprotein that requires chitin binding before binding Ca^{2+} (155). AP7 induces aragonite formation through supramolecular assemblies that include a cysteine-rich C-RING motif that is typically for Zn^{2+} binding (156, 157). AP7 does not require Zn^{2+}, suggesting that the protein instead forms a supramolecular structure via Ca^{2+} binding. Each of the acid-rich proteins from *S. pistillata* forms aragonite *in vitro*, which is distinct for corals that more commonly form calcite (158).

Other larger proteins from pearl oysters also participate in aragonite formation. Pif from *Pinctada fucata* is posttranslationally cleaved into the highly acidic Pif80 (55 kDa) and Pif97 (59.8 kDa). While bound to a chitin surface, Pif80 induces the growth of aragonite

(159). Pif97 stabilizes amorphous $CaCO_3$ and binds strongly to metastable aragonite (160). N40 (40 kDa) from *Pinctada fucata* also forms aragonite but is distinctly nonacidic and does not require posttranslational processing or binding to a fixed surface (161).

Relative to calcite formation in egg shells, less is known about the mechanisms of $CaCO_3$ formation and arrangement in aragonite-forming marine organisms. However, the small size of the proteins makes them more attractive for potential inclusion in MICP strategies.

FUTURE OPTIMIZATION OF MICP

Geotechnical aspects and other mechanical properties of biocements have been well characterized for optimization, whereas the biology of MICP has received less attention. Above, we provide the currently understood principles involved in biological $CaCO_3$ precipitation, and we illustrate the operation of those principles in *Sporosarcina pasteurii* (Fig. 2). In this section, we offer suggestions for how the observations above might drive additional optimization of the biology of MICP.

Optimizing urea entry and consumption. Before any of the targets highlighted in Fig. 2 can be fully addressed in *S. pasteurii*, genetic tools for *S. pasteurii* must be established, and genomes of additional *S. pasteurii* strains must be assembled, annotated, and published. The fully assembled genome sequence of *S. pasteurii* BNCC 337394 is deposited in the NCBI database (CP038012.1), but the genome for the commonly used type strain DSM 33 is currently deposited as two unassembled contigs (GCF_900457495.1). Moving forward, the community must prioritize sequencing, fully assembling, and thoroughly annotating genomes of all strains under intense investigation for biocementation.

With a genome sequence and genetic tools, researchers can begin where our model begins (Fig. 2) by investigating urea transport. We were unable to find reports describing urea transport or the presence of urea transporter genes in *S. pasteurii*. Future work should investigate and characterize current and future deposited genomes for known urea transport systems. If urea transport systems are indeed absent from *S. pasteurii*, systems from other organisms should be engineered for operation in *S. pasteurii*. Increasing the efficiency of urea transport could increase intracellular urea concentrations, reducing urea feedstock requirements.

The *S. pasteurii* urease (Fig. 2B), the next and maybe most immediate target, has a strikingly high K_m (17 to 300 mM) (111–113) and would particularly benefit from elevated intracellular urea concentrations that might be provided by engineered urea transport systems. Modifying or replacing the *S. pasteurii* urease to provide access to a urease with a lower K_m value would also lead to lower urea feedstock requirements. Combined with efficient urea transport, an improved urease could reduce the cost of cementation inputs without decreasing cementation strength.

Although there are no consistent quantitative values available for the V_{max} of the *S. pasteurii* urease, measured activity in cell extract is consistently $>$10,000 nmol/min/mg (100, 162). The markedly high urease activity suggests some combination of a high V_{max} and high expression levels of *ure* genes. Researchers have regularly targeted many of their studies at mutagenizing *S. pasteurii* or isolating similar bacteria to find strains with similar or higher urease activity (163, 164). However, current evidence suggests that strains with urease activity less than wild-type *S. pasteurii* induce larger $CaCO_3$ crystals and equivalent or improved $CaCO_3$ precipitation, cementation, and/or uniformity of cementation (102, 165).

Sufficient information about *S. pasteurii* urease structure is available to optimize the *S. pasteurii* enzyme (e.g., K_m and k_{cat}). Relevant residues for Ni^{2+} binding, substrate binding, and catalysis are well established (107–110). However, information about expression of *ure* genes is scarce. Early reports observed that urease activity in *S. pasteurii* was not regulated in response to urea or NH_4^+ in media (100), and two reports have observed mild regulation of *ure* gene transcripts (33, 93). In all reported cases that we found, however, few conditions were investigated, and nearly all conditions included rich complex media. Among other organisms, transcriptional control of *ure* genes varies per organism but is well established. Future work should focus on the genetics of *ure* gene expression in *S. pasteurii* with

emphasis on identifying promoters, transcriptional regulators, translational control, and the extent of the polycistronic nature of the *ure* gene cluster.

Optimizing CO_3^{2-} production and export. For optimizing biocementation, researchers must optimize processes that enable CO_3^{2-} to accumulate outside of the cell. Figure 2C and E show the potential strategies for rapidly converting HCO_3^- to CO_3^{2-} and for allowing CO_3^{2-} to accumulate outside of the cell. The most common biological strategy for equilibrating CO_2 and HCO_3^-, the enzyme carbonic anhydrase, is encoded in the *S. pasteurii* BNCC 337394 genome and has already been observed to be advantageous for MICP by *B. megaterium* and higher organisms (33, 76–78). Conversion of HCO_3^- to CO_3^{2-} is rapid and dependent on elevated pH, which is only available outside of the cell. The export strategy of CO_2/HCO_3^-/CO_3^{2-} in *S. pasteurii* is currently unknown and requires further study.

Optimizing $CaCO_3$ formation. Once CO_3^{2-} is abundant outside the cell, Fig. 2F illustrates that accumulated Ca^{2+} will interact with the CO_3^{2-} to form $CaCO_3$. Optimization of this step will require cellular modifications and/or identification of growth parameters that enhance production of structures such as teichoic acids, EPS, and TUPs. These structures vary among organisms, so the genes for biosynthesis of these structures also vary. The identity and expression of these genes for *S. pasteurii* should be characterized. Similarly, researchers should consider modifying bacteria to affix $CaCO_3$-precipitating proteins from higher organisms to the cell surface to drive efficient and morphologically specific $CaCO_3$ formation. Researchers should note that proteins such as lysozyme and ovotransferrin have antibacterial properties that should be inactivated before use in MICP.

Optimizing microbial communities for MICP. While *S. pasteurii* serves as the model bacterium for MICP, microorganisms capable of $CaCO_3$-biomineralization are diverse. Future advances in MICP can leverage this diversity for various applications based on environmental and physiological requirements of individual use cases. For instance, employing organisms that perform photosynthesis and nitrogen fixation can induce $CaCO_3$ mineralization while reducing the need for exogenous chemical MICP inputs for other members of consortia. These metabolisms can simultaneously use atmospheric CO_2 and N_2 to provide *in situ* sources of MICP inputs and nutrients for microbes performing MICP. Effective consortia might also include ureolytic fungi whose combined mycelia can contribute additional $CaCO_3$ nucleation sites and physical strength akin to fiber-reinforced concrete.

Optimizing MICP for an industrial scale. Most studies to date have focused on laboratory-scale MICP. However, in the maturation of these technologies, researchers will need to address industrial scale challenges beyond the model in Fig. 2. Using current methods, media costs are unsustainable at large scale. Several studies have explored inexpensive media options, including use of waste products from other industrial processes such as corn steep liquor (166–169), lactose mother liquor (170), waste from tofu production (171), and food-grade yeast extract (16) as primary growth substrates.

Other issues with performing MICP at scale pertain to human and environmental health. With ureolytic MICP, high concentrations of ammonia are by-products of ureolysis. Concentrated ammonia is toxic to many macroorganisms, including humans, and the environmental fate of ammonia produced by MICP has largely been unaddressed (172). Foreseeable issues include ammonium runoff into surface waters that can fuel harmful algal blooms and other ill effects on local ecosystems and fisheries. While we advocate for engineering *S. pasteurii* and/or its consortia members, we must also note that employing genetically modified organisms may hamper scale-up of MICP (173).

SUMMARY

Most of the previous work to optimize MICP has focused on optimizing treatment conditions while considering the microbes as formulation ingredients rather than biological systems (20, 21, 163). Here, we provide evidence for a model for the cellular processes and structures involved in ureolytic MICP (Fig. 2). Our model highlights many open questions regarding MICP via *S. pasteurii* and suggests paths for potential biological improvement. We hope that our model can provide to the community an investigative foundation for better understanding the fascinating physiology and environmental role of extremophilic bacteria

such as *S. pasteurii* and a foundation for producing a more sustainable and low-CO_2 alternative to traditional concrete.

REFERENCES

1. Hall C. 1976. On the history of Portland cement after 150 years. J Chem Educ 53:222. https://doi.org/10.1021/ed053p222.
2. Andrew RM. 2018. Global CO_2 emissions from cement production. Earth Syst Sci Data 10:195–217. https://doi.org/10.5194/essd-10-195-2018.
3. Lehne J, Preston F. 2018. Making concrete change innovation in low-carbon cement and concrete. Chatham House, The Royal Institute of International Affairs, London, UK.
4. Heveran CM, Williams SL, Qiu J, Artier J, Hubler MH, Cook SM, Cameron JC, Srubar WV. 2020. Biomineralization and successive regeneration of engineered living building materials. Matter 2:481–494. https://doi.org/10.1016/j.matt.2019.11.016.
5. Li Z, Zhao G, Chen J, Liu K, Xiang H, Tian Y. 2021. Growth kinetics of *Bacillus pasteurii* in solid-free drilling fluids. ACS Omega 6:25170–25178. https://doi.org/10.1021/acsomega.1c02616.
6. Phillips AJ, Troyer E, Hiebert R, Kirkland C, Gerlach R, Cunningham AB, Spangler L, Kirksey J, Rowe W, Esposito R. 2018. Enhancing wellbore cement integrity with microbially induced calcite precipitation (MICP): a field scale demonstration. J Pet Sci Eng 171:1141–1148. https://doi.org/10.1016/j.petrol.2018.08.012.
7. Li L, Li Y, Liu S, Jackson State University Department of Civil & Environmental Engineering, Maritime Transportation Research and Education Center (MarTREC). 2019. Large scale evaluation of erosion resistance of biocementation against bridge scour and roadway shoulder erosion. Jackson State University, Jackson, MS.
8. Jiang X, Rutherford C, Ikuma K, Cetin B. 2018. Use of biocementation for slope stabilization of levees—final report. US Department of Transportation Technical Report. Iowa State University Institute of Transportation, Midwest Transportation Center, US Department of Transportation, Ames, IA.
9. Fattahi SM, Soroush A, Huang N. 2020. Biocementation control of sand against wind erosion. J Geotech Geoenviron Eng 146. https://doi.org/10.1061/(ASCE)GT.1943-5606.0002268.
10. Peplow M. 2020. Bioconcrete presages new wave in environmentally friendly construction. Nat Biotechnol 38:776–778. https://doi.org/10.1038/s41587-020-0595-z.
11. Leejeerajumnean A, Ames JM, Owens JD. 2000. Effect of ammonia on the growth of *Bacillus* species and some other bacteria. Lett Appl Microbiol 30:385–389. https://doi.org/10.1046/j.1472-765x.2000.00734.x.
12. Lapierre FM, Schmid J, Ederer B, Ihling N, Büchs J, Huber R. 2020. Revealing nutritional requirements of MICP-relevant *Sporosarcina pasteurii* DSM33 for growth improvement in chemically defined and complex media. Sci Rep 10. https://doi.org/10.1038/s41598-020-79904-9.
13. Castro-Alonso MJ, Montañez-Hernandez LE, Sanchez-Muñoz MA, Macias Franco MR, Narayanasamy R, Balagurusamy N. 2019. Microbially induced calcium carbonate precipitation (MICP) and its potential in bioconcrete: microbiological and molecular concepts. Front Mater 6:126. https://doi.org/10.3389/fmats.2019.00126.
14. Hoffmann TD, Reeksting BJ, Gebhard S. 2021. Bacterium-induced mineral precipitation: a mechanistic review. Microbiology 167:001049. https://doi.org/10.1099/mic.0.001049.
15. Rusznyák A, Akob DM, Nietzsche S, Eusterhues K, Totsche KU, Neu TR, Frosch T, Popp J, Keiner R, Geletneky J, Katzschmann L, Schulze E-D, Küsel K. 2012. Calcite biomineralization by bacterial isolates from the recently discovered pristine karstic Herrenberg cave. Appl Environ Microbiol 78:1157–1167. https://doi.org/10.1128/AEM.06568-11.
16. Omoregie AI, Ong DEL, Nissom PM. 2019. Assessing ureolytic bacteria with calcifying abilities isolated from limestone caves for biocalcification. Lett Appl Microbiol 68:173–181. https://doi.org/10.1111/lam.13103.
17. Balch WM. 2018. The ecology, biogeochemistry, and optical properties of coccolithophores. Annu Rev Mar Sci 10:71–98. https://doi.org/10.1146/annurev-marine-121916-063319.
18. Zhu T, Dittrich M. 2016. Carbonate precipitation through microbial activities in natural environment, and their potential in biotechnology: a review. Front Bioeng Biotechnol 4:4. https://doi.org/10.3389/fbioe.2016.00004.
19. Boquet E, Boronat A, Ramos-Cormenzana A. 1973. Production of calcite (calcium carbonate) crystals by soil bacteria is a general phenomenon. Nature 246:527–529. https://doi.org/10.1038/246527a0.
20. Chuo SC, Mohamed SF, Mohd Setapar SH, Ahmad A, Jawaid M, Wani WA, Yaqoob AA, Mohamad Ibrahim MN. 2020. Insights into the current trends in the utilization of bacteria for microbially induced calcium carbonate precipitation. Materials 13:4993. https://doi.org/10.3390/ma13214993.
21. Pacheco VL, Bragagnolo L, Reginatto C, Thomé A. 2022. Microbially induced calcite precipitation (MICP): review from an engineering perspective. Geotech Geol Eng 40:2379–2396. https://doi.org/10.1007/s10706-021-02041-1.
22. Bansal R, Dhami NK, Mukherjee A, Reddy MS. 2016. Biocalcification by halophilic bacteria for remediation of concrete structures in marine environment. J Ind Microbiol Biotechnol 43:1497–1505. https://doi.org/10.1007/s10295-016-1835-6.
23. Rajasekar A, Moy CKS, Wilkinson S, Sekar R. 2021. Microbially induced calcite precipitation performance of multiple landfill indigenous bacteria compared to a commercially available bacteria in porous media. PLoS One 16:e0254676. https://doi.org/10.1371/journal.pone.0254676.
24. Raveh-Amit H, Tsesarsky M. 2020. Biostimulation in desert soils for microbial-induced calcite precipitation. Appl Sci 10:2905. https://doi.org/10.3390/app10082905.
25. Gat D, Ronen Z, Tsesarsky M. 2016. Soil bacteria population dynamics following stimulation for ureolytic microbial-induced $CaCO_3$ precipitation. Environ Sci Technol 50:616–624. https://doi.org/10.1021/acs.est.5b04033.
26. Fang C, Achal V. 2019. Biostimulation of calcite precipitation process by bacterial community in improving cement stabilized rammed earth as sustainable material. Appl Microbiol Biotechnol 103:7719–7727. https://doi.org/10.1007/s00253-019-10024-9.
27. Dhami NK, Alsubhi WR, Watkin E, Mukherjee A. 2017. Bacterial community dynamics and biocement formation during stimulation and augmentation: implications for soil consolidation. Front Microbiol 8:1267. https://doi.org/10.3389/fmicb.2017.01267.
28. Popall RM, Bolhuis H, Muyzer G, Sánchez-Román M. 2020. Stromatolites as biosignatures of atmospheric oxygenation: carbonate biomineralization and UV-C resilience in a *Geitlerinema* sp.-dominated culture. Front Microbiol 11:948. https://doi.org/10.3389/fmicb.2020.00948.
29. Zhu X, Li W, Zhan L, Huang M, Zhang Q, Achal V. 2016. The large-scale process of microbial carbonate precipitation for nickel remediation from an industrial soil. Environ Pollut 219:149–155. https://doi.org/10.1016/j.envpol.2016.10.047.
30. Thierstein HR, Young JR. 2004. Coccolithophores: from molecular processes to global impact. Springer, Berlin, Germany.
31. Miquel P. 1898. Etude sur la fermentation ammoniacale et sur les ferments de l'urée. Carré et Naud, Paris, France.
32. Whitman WB, Rainey F, Kämpfer P, Trujillo M, Chun J, DeVos P, Hedlund B, Dedysh S (ed). 2015. *Sporosarcina*, p 1–7. *In* Bergey's manual of systematics of archaea and bacteria. Wiley, New York, NY.
33. Ma L, Pang A-P, Luo Y, Lu X, Lin F. 2020. Beneficial factors for biomineralization by ureolytic bacterium *Sporosarcina pasteurii*. Microb Cell Fact 19:12. https://doi.org/10.1186/s12934-020-1281-z.
34. Burdalski RJ, Ribeiro BGO, Gomez MG, Gorman-Lewis D. 2022. Mineralogy, morphology, and reaction kinetics of ureolytic bio-cementation in the presence of seawater ions and varying soil materials. Sci Rep 12:17100. https://doi.org/10.1038/s41598-022-21268-3.
35. Rahman MM, Hora RN, Ahenkorah I, Beecham S, Karim MR, Iqbal A. 2020. State-of-the-art review of microbial-induced calcite precipitation and its sustainability in engineering applications. Sustainability 12:6281. https://doi.org/10.3390/su12156281.
36. Tang C-S, Yin L, Jiang N, Zhu C, Zeng H, Li H, Shi B. 2020. Factors affecting the performance of microbial-induced carbonate precipitation (MICP)-treated soil: a review. Environ Earth Sci 79:94. https://doi.org/10.1007/s12665-020-8840-9.
37. Almajed A, Lateef MA, Moghal AAB, Lemboye K. 2021. State-of-the-art review of the applicability and challenges of microbial-induced calcite precipitation (MICP) and enzyme-induced calcite precipitation (EICP) techniques for geotechnical and geoenvironmental applications. Crystals 11:370. https://doi.org/10.3390/cryst11040370.
38. Williams SL, Kirisits MJ, Ferron RD. 2016. Optimization of growth medium for *Sporosarcina pasteurii* in bio-based cement pastes to mitigate delay in hydration kinetics. J Ind Microbiol Biotechnol 43:567–575. https://doi.org/10.1007/s10295-015-1726-2.

39. Sarmast M, Farpoor MH, Sarcheshmehpoor M, Eghbal MK. 2014. Micromorphological and biocalcification effects of *Sporosarcina pasteurii* and *Sporosarcina ureae* in sandy soil columns. J Agric Sci Technol 16:681–693.
40. Bhaskar S, Anwar Hossain KM, Lachemi M, Wolfaardt G, Otini Kroukamp M. 2017. Effect of self-healing on strength and durability of zeolite-immobilized bacterial cementitious mortar composites. Cem Concr Compos 82:23–33. https://doi.org/10.1016/j.cemconcomp.2017.05.013.
41. Kim HJ, Eom HJ, Park C, Jung J, Shin B, Kim W, Chung N, Choi I-G, Park W. 2016. Calcium carbonate precipitation by *Bacillus* and *Sporosarcina* strains isolated from concrete and analysis of the bacterial community of concrete. J Microbiol Biotechnol 26:540–548. https://doi.org/10.4014/jmb.1511.11008.
42. Wei S, Cui H, Jiang Z, Liu H, He H, Fang N. 2015. Biomineralization processes of calcite induced by bacteria isolated from marine sediments. Braz J Microbiol 46:455–464. https://doi.org/10.1590/S1517-838246220140533.
43. Li M, Zhu X, Mukherjee A, Huang M, Achal V. 2017. Biomineralization in metakaolin modified cement mortar to improve its strength with lowered cement content. J Hazard Mater 329:178–184. https://doi.org/10.1016/j.jhazmat.2017.01.035.
44. Rozenbaum O, Anne S, Rouet J-L. 2014. Modification and modeling of water ingress in limestone after application of a biocalcification treatment. Constr Build Mater 70:97–103. https://doi.org/10.1016/j.conbuildmat.2014.07.038.
45. Helmi FM, Elmitwalli HR, Elnagdy SM, El-Hagrassy AF. 2016. Calcium carbonate precipitation induced by ureolytic bacteria *Bacillus licheniformis*. Ecol Eng 90:367–371. https://doi.org/10.1016/j.ecoleng.2016.01.044.
46. Dhami NK, Reddy MS, Mukherjee A. 2013. *Bacillus megaterium* mediated mineralization of calcium carbonate as biogenic surface treatment of green building materials. World J Microbiol Biotechnol 29:2397–2406. https://doi.org/10.1007/s11274-013-1408-z.
47. Sun X, Miao L. 2020. Application of bio-remediation with *Bacillus megaterium* for crack repair at low temperature. ACT 18:307–319. https://doi.org/10.3151/jact.18.307.
48. Jagannathan P, Satya Narayanan KS, Devi Arunachalam K, Kumar Annamalai S. 2018. Studies on the mechanical properties of bacterial concrete with two bacterial species. Mater Today Proc 5:8875–8879. https://doi.org/10.1016/j.matpr.2017.12.320.
49. Mondal S, Ghosh A. 2018. Investigation into the optimal bacterial concentration for compressive strength enhancement of microbial concrete. Constr Build Mater 183:202–214. https://doi.org/10.1016/j.conbuildmat.2018.06.176.
50. Qian C, Ren L, Xue B, Cao T. 2016. Bio-mineralization on cement-based materials consuming CO_2 from atmosphere. Constr Build Mater 106:126–132. https://doi.org/10.1016/j.conbuildmat.2015.10.105.
51. Chen H, Qian C, Huang H. 2016. Self-healing cementitious materials based on bacteria and nutrients immobilized respectively. Constr Build Mater 126:297–303. https://doi.org/10.1016/j.conbuildmat.2016.09.023.
52. Wang K, Qian C, Wang R. 2016. The properties and mechanism of microbial mineralized steel slag bricks. Constr Build Mater 113:815–823. https://doi.org/10.1016/j.conbuildmat.2016.03.122.
53. Jiang L, Jia G, Wang Y, Li Z. 2020. Optimization of sporulation and germination conditions of functional bacteria for concrete crack-healing and evaluation of their repair capacity. ACS Appl Mater Interfaces 12:10938–10948. https://doi.org/10.1021/acsami.9b21465.
54. Alazhari M, Sharma T, Heath A, Cooper R, Paine K. 2018. Application of expanded perlite encapsulated bacteria and growth media for self-healing concrete. Constr Build Mater 160:610–619. https://doi.org/10.1016/j.conbuildmat.2017.11.086.
55. Kumari C, Das B, Jayabalan R, Davis R, Sarkar P. 2017. Effect of nonureolytic bacteria on engineering properties of cement mortar. J Mater Civ Eng 29:06016024. https://doi.org/10.1061/(ASCE)MT.1943-5533.0001828.
56. Sharma TK, Alazhari M, Heath A, Paine K, Cooper RM. 2017. Alkaliphilic *Bacillus* species show potential application in concrete crack repair by virtue of rapid spore production and germination then extracellular calcite formation. J Appl Microbiol 122:1233–1244. https://doi.org/10.1111/jam.13421.
57. Martuscelli C, Soares C, Camões A, Lima N. 2020. Potential of fungi for concrete repair. Procedia Manuf 46:180–185. https://doi.org/10.1016/j.promfg.2020.03.027.
58. Bindschedler S, Cailleau G, Verrecchia E. 2016. Role of fungi in the biomineralization of calcite. Minerals 6:41. https://doi.org/10.3390/min6020041.
59. Li Q, Csetenyi L, Gadd GM. 2014. Biomineralization of metal carbonates by *Neurospora crassa*. Environ Sci Technol 48:14409–14416. https://doi.org/10.1021/es5042546.
60. Li Q, Csetenyi L, Paton GI, Gadd GM. 2015. $CaCO_3$ and $SrCO_3$ bioprecipitation by fungi isolated from calcareous soil: metal carbonate biomineralization by fungi. Environ Microbiol 17:3082–3097. https://doi.org/10.1111/1462-2920.12954.
61. Li T, Hu Y, Zhang B. 2018. Biomineralization induced by *Colletotrichum acutatum*: a potential strategy for cultural relic bioprotection. Front Microbiol 9:1884. https://doi.org/10.3389/fmicb.2018.01884.
62. Fang C, Kumari D, Zhu X, Achal V. 2018. Role of fungal-mediated mineralization in biocementation of sand and its improved compressive strength. Int Biodeterior Biodegrad 133:216–220. https://doi.org/10.1016/j.ibiod.2018.07.013.
63. Zhao J, Csetenyi L, Gadd GM. 2022. Fungus-induced $CaCO_3$ and $SrCO_3$ precipitation: a potential strategy for bioprotection of concrete. Sci Total Environ 816:151501. https://doi.org/10.1016/j.scitotenv.2021.151501.
64. Zhao J, Dyer T, Csetenyi L, Jones R, Gadd GM. 2022. Fungal colonization and biomineralization for bioprotection of concrete. J Clean Prod 330:129793. https://doi.org/10.1016/j.jclepro.2021.129793.
65. Ahenkorah I, Rahman MM, Karim MR, Beecham S. 2021. Enzyme induced calcium carbonate precipitation and its engineering application: a systematic review and meta-analysis. Constr Build Mater 308:125000. https://doi.org/10.1016/j.conbuildmat.2021.125000.
66. Velásquez L, Dussan J. 2009. Biosorption and bioaccumulation of heavy metals on dead and living biomass of *Bacillus sphaericus*. J Hazard Mater 167:713–716. https://doi.org/10.1016/j.jhazmat.2009.01.044.
67. Valladares A, Montesinos ML, Herrero A, Flores E. 2002. An ABC-type, high-affinity urea permease identified in cyanobacteria. Mol Microbiol 43:703–715. https://doi.org/10.1046/j.1365-2958.2002.02778.x.
68. Sebbane F, Bury-Moné S, Cailliau K, Browaeys-Poly E, De Reuse H, Simonet M. 2002. The *Yersinia pseudotuberculosis* Yut protein, a new type of urea transporter homologous to eukaryotic channels and functionally interchangeable *in vitro* with the *Helicobacter pylori* UreI protein. Mol Microbiol 45:1165–1174. https://doi.org/10.1046/j.1365-2958.2002.03096.x.
69. Cui Y, Zhou K, Strugatsky D, Wen Y, Sachs G, Zhou ZH, Munson K. 2019. pH-dependent gating mechanism of the *Helicobacter pylori* urea channel revealed by cryo-EM. Sci Adv 5:eaav8423. https://doi.org/10.1126/sciadv.aav8423.
70. Pines D, Ditkovich J, Mukra T, Miller Y, Kiefer PM, Daschakraborty S, Hynes JT, Pines E. 2016. How acidic is carbonic acid? J Phys Chem B 120:2440–2451. https://doi.org/10.1021/acs.jpcb.5b12428.
71. Sumner JB. 1926. The isolation and crystallization of the enzyme urease. J Biol Chem 69:435–441. https://doi.org/10.1016/S0021-9258(18)84560-4.
72. Bell TG, Johnson MT, Jickells TD, Liss PS. 2008. Ammonia/ammonium dissociation coefficient in seawater: a significant numerical correction. Environ Chem 5:258. https://doi.org/10.1071/EN07032_CO.
73. Jahns T. 1996. Ammonium/urea-dependent generation of a proton electrochemical potential and synthesis of ATP in *Bacillus pasteurii*. J Bacteriol 178:403–409. https://doi.org/10.1128/jb.178.2.403-409.1996.
74. Wacker T, Garcia-Celma JJ, Lewe P, Andrade SLA. 2014. Direct observation of electrogenic NH_4^+ transport in ammonium transport (Amt) proteins. Proc Natl Acad Sci U S A 111:9995–10000. https://doi.org/10.1073/pnas.1406409111.
75. Endeward V, Al-Samir S, Itel F, Gros G. 2014. How does carbon dioxide permeate cell membranes? A discussion of concepts, results and methods. Front Physiol 4:382. https://doi.org/10.3389/fphys.2013.00382.
76. Dhami NK, Reddy MS, Mukherjee A. 2014. Synergistic role of bacterial urease and carbonic anhydrase in carbonate mineralization. Appl Biochem Biotechnol 172:2552–2561. https://doi.org/10.1007/s12010-013-0694-0.
77. Gautron J, Stapane L, Le Roy N, Nys Y, Rodriguez-Navarro AB, Hincke MT. 2021. Avian eggshell biomineralization: an update on its structure, mineralogy and protein tool kit. BMC Mol Cell Biol 22:11. https://doi.org/10.1186/s12860-021-00350-0.
78. Rahman MA, Oomori T, Wörheide G. 2011. Calcite formation in soft coral sclerites is determined by a single reactive extracellular protein. J Biol Chem 286:31638–31649. https://doi.org/10.1074/jbc.M109.070185.
79. Badger MR, Price GD. 2003. CO_2 concentrating mechanisms in cyanobacteria: molecular components, their diversity and evolution. J Exp Bot 54:609–622. https://doi.org/10.1093/jxb/erg076.
80. Cordat E, Casey JR. 2009. Bicarbonate transport in cell physiology and disease. Biochem J 417:423–439. https://doi.org/10.1042/BJ20081634.
81. Dominguez DC. 2004. Calcium signalling in bacteria: calcium in bacteria. Mol Microbiol 54:291–297. https://doi.org/10.1111/j.1365-2958.2004.04276.x.
82. Naseem R, Holland IB, Jacq A, Wann KT, Campbell AK. 2008. pH and monovalent cations regulate cytosolic free Ca^{2+} in *Escherichia coli*. Biochim Biophys Acta 1778:1415–1422. https://doi.org/10.1016/j.bbamem.2008.02.006.
83. Marvasi M, Casillas-Santiago LM, Henríquez T, Casillas-Martinez L. 2017. Involvement of *etfA* gene during $CaCO_3$ precipitation in *Bacillus subtilis* biofilm. Geomicrobiol J 34:722–728. https://doi.org/10.1080/01490451.2016.1248254.

84. Achal V, Mukherjee A, Basu PC, Reddy MS. 2009. Strain improvement of *Sporosarcina pasteurii* for enhanced urease and calcite production. J Ind Microbiol Biotechnol 36:981–988. https://doi.org/10.1007/s10295-009-0578-z.
85. Bains A, Dhami NK, Mukherjee A, Reddy MS. 2015. Influence of exopolymeric materials on bacterially induced mineralization of carbonates. Appl Biochem Biotechnol 175:3531–3541. https://doi.org/10.1007/s12010-015-1524-3.
86. Zhang C, Yin L, Ou Y, Yang G, Huang L, Li F. 2021. Contribution of selective bacterial extracellular polymeric substances to the polymorphism and morphologies of formed Ca/Mg carbonates. Int Biodeterior Biodegrad 160:105213. https://doi.org/10.1016/j.ibiod.2021.105213.
87. Di Martino P. 2018. Extracellular polymeric substances, a key element in understanding biofilm phenotype. AIMS Microbiol 4:274–288. https://doi.org/10.3934/microbiol.2018.2.274.
88. Aono R, Ito M, Machida T. 1999. Contribution of the cell wall component teichuronopeptide to pH homeostasis and alkaliphily in the alkaliphile *Bacillus lentus* C-125. J Bacteriol 181:6600–6606. https://doi.org/10.1128/JB.181.21.6600-6606.1999.
89. Ghosh T, Bhaduri S, Montemagno C, Kumar A. 2019. *Sporosarcina pasteurii* can form nanoscale calcium carbonate crystals on cell surface. PLoS One 14:e0210339. https://doi.org/10.1371/journal.pone.0210339.
90. Larkin JM, Stokes JL. 1966. Isolation of psychrophilic species of *Bacillus*. J Bacteriol 91:1667–1671. https://doi.org/10.1128/jb.91.5.1667-1671.1966.
91. Gibson T. 1934. An investigation of the *Bacillus pasteuri* group. I. Description of strains isolated from soils and manures. J Bacteriol 28:295–311. https://doi.org/10.1128/jb.28.3.295-311.1934.
92. Bornside GH, Kallio RE. 1956. Urea-hydrolyzing bacilli II. J Bacteriol 71:655–660. https://doi.org/10.1128/jb.71.6.655-660.1956.
93. Pei D, Liu Z, Wu W, Hu B. 2021. Transcriptome analyses reveal the utilization of nitrogen sources and related metabolic mechanisms of *Sporosarcina pasteurii*. PLoS One 16:e0246818. https://doi.org/10.1371/journal.pone.0246818.
94. Ip YK, Chew SF, Randall DJ. 2001. Ammonia toxicity, tolerance, and excretion, p 109–148. *In* Fish physiology. Academic Press, Inc, New York, NY.
95. Braissant O, McLin VA, Cudalbu C. 2013. Ammonia toxicity to the brain. J Inherit Metab Dis 36:595–612. https://doi.org/10.1007/s10545-012-9546-2.
96. Vines HM, Wedding RT. 1960. Some effects of ammonia on plant metabolism and a possible mechanism for ammonia toxicity. Plant Physiol 35:820–825. https://doi.org/10.1104/pp.35.6.820.
97. Hoffmann TD, Paine K, Gebhard S. 2021. Genetic optimization of bacterium-induced calcite precipitation in *Bacillus subtilis*. Microb Cell Factories 20. https://doi.org/10.1186/s12934-021-01704-1.
98. Preiss L, Hicks DB, Suzuki S, Meier T, Krulwich TA. 2015. Alkaliphilic bacteria with impact on industrial applications, concepts of early life forms, and bioenergetics of ATP synthesis. Front Bioeng Biotechnol 3:75. https://doi.org/10.3389/fbioe.2015.00075.
99. Matsuno T, Goto T, Ogami S, Morimoto H, Yamazaki K, Inoue N, Matsuyama H, Yoshimune K, Yumoto I. 2018. Formation of proton motive force under low-aeration alkaline conditions in alkaliphilic bacteria. Front Microbiol 9:2331. https://doi.org/10.3389/fmicb.2018.02331.
100. Mörsdorf G, Kaltwasser H. 1989. Ammonium assimilation in *Proteus vulgaris*, *Bacillus pasteurii*, and *Sporosarcina ureae*. Arch Microbiol 152:125–131. https://doi.org/10.1007/BF00456089.
101. Liang L, Heveran C, Liu R, Gill RT, Nagarajan A, Cameron J, Hubler M, Srubar WV, Cook SM. 2018. Rational control of calcium carbonate precipitation by engineered *Escherichia coli*. ACS Synth Biol 7:2497–2506. https://doi.org/10.1021/acssynbio.8b00194.
102. Heveran CM, Liang L, Nagarajan A, Hubler MH, Gill R, Cameron JC, Cook SM, Srubar WV. 2019. Engineered ureolytic microorganisms can tailor the morphology and nanomechanical properties of microbial-precipitated calcium carbonate. Sci Rep 9:14721. https://doi.org/10.1038/s41598-019-51133-9.
103. Mols M, Abee T. 2008. Role of ureolytic activity in *Bacillus cereus* nitrogen metabolism and acid survival. Appl Environ Microbiol 74:2370–2378. https://doi.org/10.1128/AEM.02737-07.
104. Pearson MM, Yep A, Smith SN, Mobley HLT. 2011. Transcriptome of *Proteus mirabilis* in the murine urinary tract: virulence and nitrogen assimilation gene expression. Infect Immun 79:2619–2631. https://doi.org/10.1128/IAI.05152-11.
105. Sachs G, Scott DR, Weeks DL, Rektorscheck M, Melchers K. 2001. Regulation of urease for acid habitation. *In* Mobley HL, Mendz GL, Hazell SL (ed), *Helicobacter pylori*: physiology and genetics. ASM Press, Washington, DC.
106. Benini S, Ciurli S, Rypniewski WR, Wilson KS, Mangani S. 1998. Crystallization and preliminary high-resolution X-ray diffraction analysis of native and β-mercaptoethanol-inhibited urease from *Bacillus pasteurii*. Acta Crystallogr D Biol Crystallogr 54:409–412. https://doi.org/10.1107/s0907444997013085.
107. Mazzei L, Cianci M, Benini S, Ciurli S. 2019. The structure of the elusive urease-urea complex unveils the mechanism of a paradigmatic nickel-dependent enzyme. Angew Chem Int Ed Engl 58:7415–7419. https://doi.org/10.1002/anie.201903565.
108. Krajewska B. 2009. Ureases I. Functional, catalytic, and kinetic properties: a review. J Mol Catal B Enzym 59:9–21. https://doi.org/10.1016/j.molcatb.2009.01.003.
109. Jabri E, Carr MB, Hausinger RP, Karplus PA. 1995. The crystal structure of urease from *Klebsiella aerogenes*. Science 268:998–1004. https://doi.org/10.1126/science.7754395.
110. Pearson MA, Park I-S, Schaller RA, Michel LO, Karplus PA, Hausinger RP. 2000. Kinetic and structural characterization of urease active site variants. Biochemistry 39:8575–8584. https://doi.org/10.1021/bi000613o.
111. Bachmeier KL, Williams AE, Warmington JR, Bang SS. 2002. Urease activity in microbiologically induced calcite precipitation. J Biotechnol 93:171–181. https://doi.org/10.1016/s0168-1656(01)00393-5.
112. Larson AD, Kallio RE. 1954. Purification and properties of bacterial urease. J Bacteriol 68:67–73. https://doi.org/10.1128/jb.68.1.67-73.1954.
113. Ciurli S, Marzadori C, Benini S, Deiana S, Gessa C. 1996. Urease from the soil bacterium *Bacillus pasteurii*: immobilization on Ca-polygalacturonate. Soil Biol Biochem 28:811–817. https://doi.org/10.1016/0038-0717(96)00020-X.
114. Yang L, Wang S, Tian Y. 2010. Purification, properties, and application of a novel acid urease from *Enterobacter* sp. Appl Biochem Biotechnol 160:303–313. https://doi.org/10.1007/s12010-008-8159-6.
115. Gang JG, Yun SK, Hwang SY. 2009. *Helicobacter pylori* urease may exist in two forms: evidence from the kinetic studies. J Microbiol Biotechnol 19:1565–1568. https://doi.org/10.4014/jmb.0906.06021.
116. Lauchnor EG, Topp DM, Parker AE, Gerlach R. 2015. Whole-cell kinetics of ureolysis by *Sporosarcina pasteurii*. J Appl Microbiol 118:1321–1332. https://doi.org/10.1111/jam.12804.
117. Mahanty B, Kim S, Kim CG. 2014. Biokinetic modeling of ureolysis in *Sporosarcina pasteurii* and its integration into a numerical chemodynamic biocalcification model. Chem Geol 383:13–25. https://doi.org/10.1016/j.chemgeo.2014.05.034.
118. Connolly J, Kaufman M, Rothman A, Gupta R, Redden G, Schuster M, Colwell F, Gerlach R. 2013. Construction of two ureolytic model organisms for the study of microbially induced calcium carbonate precipitation. J Microbiol Methods 94:290–299. https://doi.org/10.1016/j.mimet.2013.06.028.
119. Graddy CMR, Gomez MG, Kline LM, Morrill SR, DeJong JT, Nelson DC. 2018. Diversity of *Sporosarcina*-like bacterial strains obtained from meter-scale augmented and stimulated biocementation experiments. Environ Sci Technol 52:3997–4005. https://doi.org/10.1021/acs.est.7b04271.
120. Hervás AB, Canosa I, Little R, Dixon R, Santero E. 2009. NtrC-dependent regulatory network for nitrogen assimilation in *Pseudomonas putida*. J Bacteriol 191:6123–6135. https://doi.org/10.1128/JB.00744-09.
121. Macaluso A, Best EA, Bender RA. 1990. Role of the *nac* gene product in the nitrogen regulation of some NTR-regulated operons of *Klebsiella aerogenes*. J Bacteriol 172:7249–7255. https://doi.org/10.1128/jb.172.12.7249-7255.1990.
122. Masepohl B, Kaiser B, Isakovic N, Richard CL, Kranz RG, Klipp W. 2001. Urea utilization in the phototrophic bacterium *Rhodobacter capsulatus* is regulated by the transcriptional activator NtrC. J Bacteriol 183:637–643. https://doi.org/10.1128/JB.183.2.637-643.2001.
123. Bender RA. 1991. The role of the NAC protein in the nitrogen regulation of *Klebsiella aerogenes*. Mol Microbiol 5:2575–2580. https://doi.org/10.1111/j.1365-2958.1991.tb01965.x.
124. Hirschman J, Wong PK, Sei K, Keener J, Kustu S. 1985. Products of nitrogen regulatory genes *ntrA* and *ntrC* of enteric bacteria activate *glnA* transcription *in vitro*: evidence that the *ntrA* product is a sigma factor. Proc Natl Acad Sci U S A 82:7525–7529. https://doi.org/10.1073/pnas.82.22.7525.
125. Liu Q, Bender RA. 2007. Complex regulation of urease formation from the two promoters of the *ure* operon of *Klebsiella pneumoniae*. J Bacteriol 189:7593–7599. https://doi.org/10.1128/JB.01096-06.
126. Wray LV, Ferson AE, Fisher SH. 1997. Expression of the *Bacillus subtilis ureABC* operon is controlled by multiple regulatory factors including CodY, GlnR, TnrA, and Spo0H. J Bacteriol 179:5494–5501. https://doi.org/10.1128/jb.179.17.5494-5501.1997.
127. Atkinson MR, Fisher SH. 1991. Identification of genes and gene products whose expression is activated during nitrogen-limited growth in *Bacillus subtilis*. J Bacteriol 173:23–27. https://doi.org/10.1128/jb.173.1.23-27.1991.

128. Ševčík R, Šašek P, Viani A. 2018. Physical and nanomechanical properties of the synthetic anhydrous crystalline $CaCO_3$ polymorphs: vaterite, aragonite and calcite. J Mater Sci 53:4022–4033. https://doi.org/10.1007/s10853-017-1884-x.
129. Falini G, Albeck S, Weiner S, Addadi L. 1996. Control of aragonite or calcite polymorphism by mollusk shell macromolecules. Science 271:67–69. https://doi.org/10.1126/science.271.5245.67.
130. Mann K. 2015. The calcified eggshell matrix proteome of a songbird, the zebra finch (*Taeniopygia guttata*). Proteome Sci 13:29. https://doi.org/10.1186/s12953-015-0086-1.
131. Mann K, Mann M. 2015. Proteomic analysis of quail calcified eggshell matrix: a comparison to chicken and turkey eggshell proteomes. Proteome Sci 13:22. https://doi.org/10.1186/s12953-015-0078-1.
132. Mann K, Gautron J, Nys Y, McKee MD, Bajari T, Schneider WJ, Hincke MT. 2003. Disulfide-linked heterodimeric clusterin is a component of the chicken eggshell matrix and egg white. Matrix Biol 22:397–407. https://doi.org/10.1016/s0945-053x(03)00072-6.
133. Marie P, Labas V, Brionne A, Harichaux G, Hennequet-Antier C, Rodriguez-Navarro AB, Nys Y, Gautron J. 2015. Quantitative proteomics provides new insights into chicken eggshell matrix protein functions during the primary events of mineralization and the active calcification phase. J Proteomics 126:140–154. https://doi.org/10.1016/j.jprot.2015.05.034.
134. Stapane L, Le Roy N, Ezagal J, Rodriguez-Navarro AB, Labas V, Combes-Soia L, Hincke MT, Gautron J. 2020. Avian eggshell formation reveals a new paradigm for vertebrate mineralization via vesicular amorphous calcium carbonate. J Biol Chem 295:15853–15869. https://doi.org/10.1074/jbc.RA120.014542.
135. Mikšík I, Eckhardt A, Sedláková P, Mikulikova K. 2007. Proteins of insoluble matrix of avian (*Gallus gallus*) eggshell. Connect Tissue Res 48:1–8. https://doi.org/10.1080/03008200601003116.
136. Kaweewong K, Garnjanagoonchorn W, Jirapakkul W, Roytrakul S. 2013. Solubilization and identification of hen eggshell membrane proteins during different times of chicken embryo development using the proteomic approach. Protein J 32:297–308. https://doi.org/10.1007/s10930-013-9487-0.
137. Jonchère V, Brionne A, Gautron J, Nys Y. 2012. Identification of uterine ion transporters for mineralization precursors of the avian eggshell. BMC Physiol 12:10. https://doi.org/10.1186/1472-6793-12-10.
138. Hincke MT. 1995. Ovalbumin is a component of the chicken eggshell matrix. Connect Tissue Res 31:227–233. https://doi.org/10.3109/03008209509010814.
139. Pipich V, Balz M, Wolf SE, Tremel W, Schwahn D. 2008. Nucleation and growth of $CaCO_3$ mediated by the egg-white protein ovalbumin: a time-resolved *in situ* study using small-angle neutron scattering. J Am Chem Soc 130:6879–6892. https://doi.org/10.1021/ja801798h.
140. Wang X, Sun H, Xia Y, Chen C, Xu H, Shan H, Lu JR. 2009. Lysozyme mediated calcium carbonate mineralization. J Colloid Interface Sci 332:96–103. https://doi.org/10.1016/j.jcis.2008.12.055.
141. Wang X, Wu C, Tao K, Zhao K, Wang J, Xu H, Xia D, Shan H, Lu JR. 2010. Influence of ovalbumin on $CaCO_3$ precipitation during *in vitro* biomineralization. J Phys Chem B 114:5301–5308. https://doi.org/10.1021/jp1008237.
142. Voinescu AE, Touraud D, Lecker A, Pfitzner A, Kunz W, Ninham BW. 2007. Mineralization of $CaCO_3$ in the presence of egg white lysozyme. Langmuir 23:12269–12274. https://doi.org/10.1021/la701892v.
143. Gautron J, Hincke MT, Panheleux M, Garcia-Ruiz JM, Boldicke T, Nys Y. 2001. Ovotransferrin is a matrix protein of the hen eggshell membranes and basal calcified layer. Connect Tissue Res 42:255–267. https://doi.org/10.3109/03008200109016840.
144. Song W, Bahn SY, Cha HJ, Pack SP, Choi YS. 2016. Recombinant production of a shell matrix protein in *Escherichia coli* and its application to the biomimetic synthesis of spherulitic calcite crystals. Biotechnol Lett 38:809–816. https://doi.org/10.1007/s10529-016-2039-x.
145. Son C, Kim SY, Bahn SY, Cha HJ, Choi YS. 2017. $CaCO_3$ thin-film formation mediated by a synthetic protein-lysozyme coacervate. RSC Adv 7:15302–15308. https://doi.org/10.1039/C6RA28808A.
146. Evans JS. 2012. Aragonite-associated biomineralization proteins are disordered and contain interactive motifs. Bioinformatics 28:3182–3185. https://doi.org/10.1093/bioinformatics/bts604.
147. Bauerlein E, Behrens P, Epple M. 2007. Handbook of biomineralization: biological aspects and structure formation. Wiley, New York, NY.
148. Song X, Liu Z, Wang L, Song L. 2019. Recent advances of shell matrix proteins and cellular orchestration in marine molluscan shell biomineralization. Front Mar Sci 6:41. https://doi.org/10.3389/fmars.2019.00041.
149. Samata T, Hayashi N, Kono M, Hasegawa K, Horita C, Akera S. 1999. A new matrix protein family related to the nacreous layer formation of *Pinctada fucata*. FEBS Lett 462:225–229. https://doi.org/10.1016/s0014-5793(99)01387-3.
150. Perovic I, Mandal T, Evans JS. 2013. A pearl protein self-assembles to form protein complexes that amplify mineralization. Biochemistry 52:5696–5703. https://doi.org/10.1021/bi400808j.
151. Kono M, Hayashi N, Samata T. 2000. Molecular mechanism of the nacreous layer formation in *Pinctada maxima*. Biochem Biophys Res Commun 269:213–218. https://doi.org/10.1006/bbrc.2000.2274.
152. Rivera-Perez C, Flores-Sánchez IA, Ojeda Ramírez de Areyano JJ, Rojas Posadas DI, Hernández-Saavedra NY. 2020. A shell matrix protein of *Pinctada mazatlanica* produces nacre platelets *in vitro*. Sci Rep 10:20201. https://doi.org/10.1038/s41598-020-77320-7.
153. Montagnani C, Marie B, Marin F, Belliard C, Riquet F, Tayalé A, Zanella-Cléon I, Fleury E, Gueguen Y, Piquemal D, Cochennec-Laureau N. 2011. Pmarg-Pearlin is a matrix protein involved in nacre framework formation in the pearl oyster *Pinctada margaritifera*. Chembiochem 12:2033–2043. https://doi.org/10.1002/cbic.201100216.
154. Amos FF, Destine E, Ponce CB, Evans JS. 2010. The N- and C-terminal regions of the pearl-associated EF hand protein, PFMG1, promote the formation of the aragonite polymorph *in vitro*. Cryst Growth Des 10:4211–4216. https://doi.org/10.1021/cg100363m.
155. Arroyo-Loranca RG, Hernandez-Saavedra NY, Hernandez-Adame L, Rivera-Perez C. 2020. Ps19, a novel chitin binding protein from *Pteria sterna* capable to mineralize aragonite plates *in vitro*. PLoS One 15:e0230431. https://doi.org/10.1371/journal.pone.0230431.
156. Amos FF, Evans JS. 2009. AP7, a partially disordered pseudo C-RING protein, is capable of forming stabilized aragonite *in vitro*. Biochemistry 48:1332–1339. https://doi.org/10.1021/bi802148r.
157. Amos FF, Ndao M, Ponce CB, Evans JS. 2011. A C-RING-like domain participates in protein self-assembly and mineral nucleation. Biochemistry 50:8880–8887. https://doi.org/10.1021/bi201346d.
158. Mass T, Drake JL, Haramaty L, Kim JD, Zelzion E, Bhattacharya D, Falkowski PG. 2013. Cloning and characterization of four novel coral acid-rich proteins that precipitate carbonates *in vitro*. Curr Biol 23:1126–1131. https://doi.org/10.1016/j.cub.2013.05.007.
159. Bahn SY, Jo BH, Choi YS, Cha HJ. 2017. Control of nacre biomineralization by Pif80 in pearl oyster. Sci Adv 3:e1700765. https://doi.org/10.1126/sciadv.1700765.
160. Bahn SY, Jo BH, Hwang BH, Choi YS, Cha HJ. 2015. Role of Pif97 in nacre biomineralization: *in vitro* characterization of recombinant Pif97 as a framework protein for the association of organic–inorganic layers in Nacre. Cryst Growth Des 15:3666–3673. https://doi.org/10.1021/acs.cgd.5b00275.
161. Yan Z, Jing G, Gong N, Li C, Zhou Y, Xie L, Zhang R. 2007. N40, a novel nonacidic matrix protein from pearl oyster Nacre, facilitates nucleation of aragonite *in vitro*. Biomacromolecules 8:3597–3601. https://doi.org/10.1021/bm0701494.
162. Christians S, Kaltwasser H. 1986. Nickel-content of urease from *Bacillus pasteurii*. Arch Microbiol 145:51–55. https://doi.org/10.1007/BF00413026.
163. Reeksting BJ, Hoffmann TD, Tan L, Paine K, Gebhard S. 2020. In-depth profiling of calcite precipitation by environmental bacteria reveals fundamental mechanistic differences with relevance to application. Appl Environ Microbiol 86:e02739-19. https://doi.org/10.1128/AEM.02739-19.
164. Šovljanski O, Pezo L, Stanojev J, Bajac B, Kovač S, Tóth E, Ristić I, Tomić A, Ranitović A, Cvetković D, Markov S. 2021. Comprehensive profiling of microbiologically induced $CaCO_3$ precipitation by ureolytic *Bacillus* isolates from alkaline soils. Microorganisms 9:1691. https://doi.org/10.3390/microorganisms9081691.
165. Konstantinou C, Wang Y, Biscontin G, Soga K. 2021. The role of bacterial urease activity on the uniformity of carbonate precipitation profiles of bio-treated coarse sand specimens. Sci Rep 11:6161. https://doi.org/10.1038/s41598-021-85712-6.
166. Achal V, Mukherjee A, Reddy MS. 2010. Biocalcification by *Sporosarcina pasteurii* using corn steep liquor as the nutrient source. Ind Biotechnol 6:170–174. https://doi.org/10.1089/ind.2010.6.170.
167. Babakhani S, Fahmi A, Katebi H, Ouria A, Majnouni-Toutakhane A, Ganbarov K, Kafil HS. 2021. Non-sterile corn steep liquor a novel, cost effective and powerful culture media for *Sporosarcina pasteurii* cultivation for sand improvement. J Appl Microbiol 130:1232–1244. https://doi.org/10.1111/jam.14866.
168. Joshi S, Goyal S, Reddy MS. 2018. Corn steep liquor as a nutritional source for biocementation and its impact on concrete structural properties. J Ind Microbiol Biotechnol 45:657–667. https://doi.org/10.1007/s10295-018-2050-4.
169. Maleki-Kakelar M, Azarhoosh MJ, Golmohammadi Senji S, Aghaeinejad-Meybodi A. 2022. Urease production using corn steep liquor as a low-

cost nutrient source by *Sporosarcina pasteurii*: biocementation and process optimization via artificial intelligence approaches. Environ Sci Pollut Res Int 29:13767–13781. https://doi.org/10.1007/s11356-021-16568-6.
170. Achal V, Mukherjee A, Basu PC, Reddy MS. 2009. Lactose mother liquor as an alternative nutrient source for microbial concrete production by *Sporosarcina pasteurii*. J Ind Microbiol Biotechnol 36:433–438. https://doi.org/10.1007/s10295-008-0514-7.
171. Fang C, He J, Achal V, Plaza G. 2019. Tofu wastewater as efficient nutritional source in biocementation for improved mechanical strength of cement mortars. Geomicrobiol J 36:515–521. https://doi.org/10.1080/01490451.2019.1576804.
172. Lee M, Gomez MG, San Pablo ACM, Kolbus CM, Graddy CMR, DeJong JT, Nelson DC. 2019. Investigating ammonium by-product removal for ureolytic bio-cementation using meter-scale experiments. Sci Rep 9:18313. https://doi.org/10.1038/s41598-019-54666-1.
173. Ivanov V, Stabnikov V, Stabnikova O, Kawasaki S. 2019. Environmental safety and biosafety in construction biotechnology. World J Microbiol Biotechnol 35:26. https://doi.org/10.1007/s11274-019-2598-9.